IEEE Access
Multidisciplinary ⋮ Rapid Review ⋮ Open Access Journal

Received 4 February 2024, accepted 15 March 2024, date of publication 25 March 2024, date of current version 12 April 2024.

Digital Object Identifier 10.1109/ACCESS.2024.3381198

RESEARCH ARTICLE

Isolated High Step-Up Soft-Switching Quasi-Z-Source DC–DC Converter

GUOSHENG TIAN[1], SHUO CHEN[1], XINPING DING[2], (Member, IEEE), JISHEN PENG[1], AND ZHUANGZHUANG KOU[2]

[1]Faculty of Electrical and Control Engineering, Liaoning Technical University, Huludao 125105, China
[2]School of Automation, Nanjing University of Information Science and Technology, Nanjing 210044, China

Corresponding author: Xinping Ding (dxinping@nuist.edu.cn)

This work was supported by the National Natural Science Foundation of China under Grant 52104160.

ABSTRACT The DC microgrid with energy storage cells has strong stability, simple control, and a convenient power supply for DC loads, increasingly becoming the grid-connected structure of distributed generation systems. This paper presents an isolated high voltage gain soft-switching dc-dc converter suitable for DC microgrid applications. The converter comprises a dual-switch quasi-z-source network, multiplier voltage cell, and transformer. It has advantages such as high voltage gain, zero voltage switching (ZVS) of switches, zero voltage zero current switching (ZVZCS) turn-on and turn-off of diodes, and low input ripple current. The converter can achieve high voltage gain with an appropriate duty cycle and transformer turns ratio, reducing leakage inductance of transformer, which decreases the power loss and voltage spike of switch. Soft-switching of active devices increases the efficiency and decreases the output voltage ripples of the converter. The steady-state characteristics of the converter, voltage and current stress of components, the efficiency of the converter, and the selection of converter parameters are analyzed in detail. Finally, a 200 W experimental prototype is built in the laboratory for experimental verification, and the experimental results are consistent with the theoretical analysis.

INDEX TERMS Isolated dc-dc converter, high-efficiency, high step-up, quasi-Z-source.

I. INTRODUCTION

With the widespread application of renewable energy, the demand for high voltage gain dc-dc converters in photovoltaic power generation systems, fuel cell systems, and semiconductor industries has increased. The DC microgrid has been increasingly accepted by both industry and academia due to its outstanding advantages. In grid-connected DC microgrids, the photovoltaic power generation system must be isolated from the AC grid to meet the safety requirements of the grid-connected system [1]. There are three isolation schemes in the existing grid-connected photovoltaic power generation system [2]: 1) Firstly, non-isolated dc-dc converters are used to boost voltage and achieve maximum power point tracking (MPPT) control [3], [4]. Then, central inverter and low-frequency transformer realize isolation and grid connection; 2) Non-isolated dc-dc converters are used to boost voltage and achieve MPPT control. Next, solid-state transformers are employed to replace central inverters and low-frequency transformers to realize inversion and isolation [5], [6]; 3) Isolated boost dc-dc converters in each photovoltaic module are utilized for isolation and voltage boost [7], [8], [9], and then central inverters are used for grid connection. The use of low-frequency transformers in the first scheme results in low power density in the system. In the second scheme, solid-state transformers reduce the volume and weight of the low-frequency transformer used in the first scheme, and the power density is significantly improved. However, power converters connected in series in solid-state transformers reduce the reliability and efficiency of the system. In contrast, the third scheme employs small-sized high-frequency transformers, reducing the size, weight, and costs of the system, and this scheme is more efficient and reliable than the other two schemes.

Since the single-stage isolated high voltage gain dc-dc converter has a simple structure and high efficiency, it has

The associate editor coordinating the review of this manuscript and approving it for publication was Liu Hongchen.

become a research hotspot in recent years [10], [11]. Isolated dc-dc converters based on full-bridge and half-bridge structures are mainly employed for high-power applications owing to their multiple switches [12], [13], [14], [15]. Conversely, single-switch converters and dual-switch converters have significant advantages for low-power applications [16], [17], [18], [19], [20]. The low-power isolated high voltage gain dc-dc converter for photovoltaic power generation requires meeting the following functions.

1) Soft switching: high voltage gain dc-dc converters need soft switching to reduce switching losses and voltage overshoots to achieve high efficiency and improve the electromagnetic environment [21], [22], [23].

2) Low input current ripple: Dc-dc converters must have low input current ripple to reduce the impulse current in photovoltaic cell modules and extend the service life of photovoltaic cell modules and converters [24], [25], [26].

3) Few components in the converter: Relatively fewer components in the converter are beneficial to the high reliability and high-power density of the system, and this is also beneficial to the size, weight, and costs [27], [28].

The simplest isolated high voltage gain dc-dc converters are single-switch converters, such as Flyback converter and Forward converter. However, when these converters achieve high voltage gain, a relatively large turns ratio of a transformer reduces efficiency and increases leakage inductance in the transformer. Furthermore, a relatively large leakage inductance of a transformer reduces converter efficiency and increases voltage overshoots across a switch. Snubber circuits and soft switching can partly remove negative effects caused by the leakage inductance of a transformer [31], [32]. However, snubber circuits and the added soft-switching circuits increase the complexity of the converter, and the input current of this type of converter is discontinuous, which has a relatively great impact on photovoltaic modules. The dual-switch zero voltage switching (ZVS) flyback converter has a relatively high voltage gain [32], but the input current is discontinuous, and the voltage stress across output diodes is high. Reference [33] proposed a soft-switching single-switch Flyback converter. The passive lossless circuit recycles the energy of leakage inductance, and the resonant network increases the voltage of switch and the voltage stress across diodes.

The current-source resonant converter can achieve high voltage gain, low current ripple, and soft switching [34], [35]. The leakage inductance of a transformer as a parameter of resonant networks is involved in the operating mode of a converter, which is a relatively ideal low-power dc-dc converter. However, the voltage stress across output diodes in these converters is relatively high and equals the output voltage of converters.

Reference [16] presented a high voltage gain dc-dc converter using voltage lift technology. This converter can recycle the energy of leakage inductance, and clamping circuits reduce voltage overshoots across switches. However, it has a relatively high input ripple current and does not have soft switching. Reference [36] investigated an isolated high voltage gain zero-voltage zero-current condition (ZVSZCS) soft-switching dc-dc converter with low input ripple current, which meets the four functions of dc-dc converters required in DC microgrids. However, the voltage gain should be further increased.

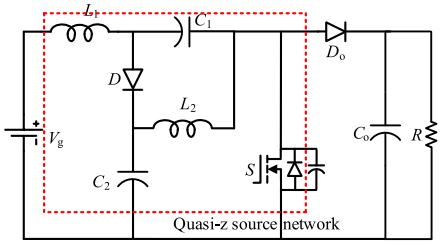

FIGURE 1. Quasi-z source Boost converter.

This paper presents a novel high-efficiency high voltage gain current-source dc-dc converter with soft-switching. The structure of the converter consists of a quasi-Z-Source network, transformers, and multiplier voltage cells. After replacing diodes with switch in the quasi-Z-Source network, all soft switching conditions of active devices can be achieved by controlling the dead time of switches and the resonance of parasitic parameters. The switches can achieve ZVS turn-on, and all diodes can achieve ZVZCS turn-on and ZVZCS turn-off. The converter has few components, low input ripple current, and high efficiency, and it is relatively suitable for DC microgrids.

II. ISOLATED HIGH VOLTAGE GAIN SOFT-SWITCHING QUASI-Z-SOURCE DC-DC CONVERTER

Fig. 1 shows a conventional quasi-Z-source Boost converter. Compared with traditional Boost converters, it continues the advantages of continuous input current and increases the voltage gain from 1/1-D to 1/1-2 D. Although its voltage gain is higher at the same duty cycle, its voltage boost capacity is still insufficient, and the switching tube works under hard switching conditions.

The Boost capacity of the traditional Z-source Boost converter is still insufficient, so the switched capacitor voltage doubling unit is extended to the Z-source boost converter. Fig 2 shows the expansion structure of the converter.

Fig. 3 shows the proposed isolated high efficiency high step-up dc-dc converter, which consists of a quasi-Z-source network, a transformer, and a voltage multiplier cell. All the active devices are operated in soft-switching condition, and the leakage inductance energy of the transformer is recycled to capacitors C_1-C_4, thereby improving the efficiency of the converter.

To simplify the analysis of the operating process, we made the following assumptions during one switching cycle.

1) All the switches and diodes are regarded as ideal; only the parasitic capacitor and body diode of the switches are considered.

2) All the capacitors C_1, C_2, C_3, C_4, and C_o are sufficiently large that the capacitor voltage remains constant.

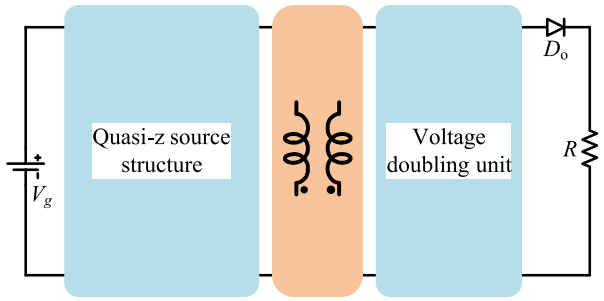

FIGURE 2. The extended structure of the converter.

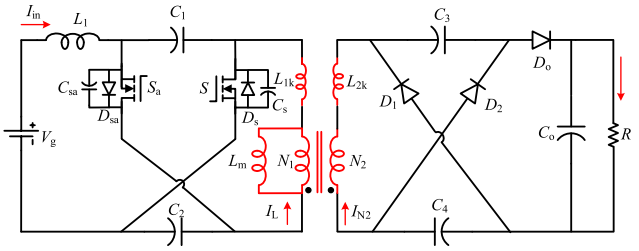

FIGURE 3. Proposed isolated high efficiency high voltage gain soft-switching quasi-Z-Source dc-dc converter.

3) The magnetizing inductance L_m and leakage inductance L_k of the transformer is considered in the analysis.

The analysis of the operating modes under continuous conduction mode (CCM) is presented in detail, while discontinuous conduction mode (DCM) is less used in the application of renewable energy.

The key waveforms of the components in one switching cycle are shown in Fig. 4. The proposed converter has seven operating modes in one switching cycle considering the leakage inductance of the transformer. The detailed operating modes are shown in Fig. 5. The current polarity of the input inductor and the windings of the transformer are shown in Fig. 3.

Prior to mode I, diodes D_o, D_1, and D_2 are reversed-biased, the switch S_a is in on-state, and the switch S is off. The input source V_g, capacitor C_1, and input inductor L_1 work together to provide energy to the capacitor C_2 and magnetizing inductor L_m, the magnetizing inductance current i_{Lm} rises linearly.

Mode *I* [t_0-t_1]. The mode starts at t_0, the control signal v_{Gsa} changes from high to low level and S_a turned off with zero voltage switching due to the snubber capacitor C_{Sa}. The input voltage V_g and capacitor C_1 transfer energy to input inductor L_1 and capacitor C_2, therefore the input current i_{L1} rises linearly. The diodes D_o, D_1, and D_2 are reverse-biased. The snubber capacitor C_S and C_{Sa} resonate with the transformer's primary side leakage inductance L_{1k}. The snubber capacitor C_{Sa} is charged, while C_S is discharged. The voltage across diodes D_1 and D_2 is equal to V_{C4}-n(V_{C2}-V_{CS}). In this mode, the diode voltages v_{D1} and v_{D1} decreases to zero. When the snubber capacitor C_S voltage resonates to zero, the body diode of the switch S is turns on because there is still reverse current on the transformer leakage inductance L_{1k}.

Mode *II* [t_1-t_2]. At t_1, switch Sa is still in off state, the body diode D_S of the main switch S is on, which clamps the voltage of the switch S to zero. The voltage on the auxiliary switch Sa is clamped to $V_{C1} + V_{C2}$ by capacitors C_1 and C_2. At the same time, the voltage across the primary winding of the transformer is clamped at V_{C2}. Hence diodes D_1 and D_2 turns on results from forward bias voltage, while diode D_o is still reverse biased. Capacitor C_1 is discharging, input inductor L_1 and capacitors C_2, C_3 and C_4 are charging. Capacitors C_3 and C_4 resonate with the secondary leakage inductance L_{2k}, diodes D_1 and D_2 are switched on under the condition of zero-voltage zero-current condition (ZVZCS). The mode ends when the current flowing through the body diode DS of switch S decreases to zero.

Mode *III* [t_2-t_3]. The mode starts at t_2, switch S turns on with ZVS due to the body diode D_S clamp the switch voltage V_S to zero. The input inductor L_1 and capacitors C_3 and C_4 receive energy from the capacitors C_1 and C_2 as well as from the input. The negative magnetizing inductance current i_{Lm} decreases to zero, then i_{Lm} reverses its direction and increases gradually. The leakage inductance L_{2k} continues to resonate with capacitor C_3 and C_4, the leakage inductance current i_{L2k} and capacitor voltage are

$$i_{L2k}(t) = \frac{V_{C3(t=t_1)} - V_{C2(t=t_1)}}{Z_0} \sin \omega_0 (t - t_1) \tag{1}$$

$$V_{C3}(t) = V_{C2(t=t_1)} + (V_{C3(t=t_1)} - V_{C2(t=t_1)}) \cos \omega_0 (t - t_1) \tag{2}$$

where $\omega_0 = \frac{1}{\sqrt{L_{2k}(C_3+C_4)}}$ and $Z_0 = \sqrt{\frac{L_{2k}}{C_3+C_4}}$

The mode ends at t_3, when the leakage inductance current i_{L2k} decreases to zero. The interval duration is half the resonate period T_0, which is

$$t_3 - t_1 = \frac{T_0}{2} = \pi \sqrt{L_{2k}(C_3 + C_4)} \tag{3}$$

Mode *IV* [t_3-t_4]. In this mode, the snubber capacitor C_S is charged, then voltage across switch S increases from 0 to VCS gradually. Thus, the switch S turns off under zero-voltage condition. The diodes D_1, D_2 turn off naturally, which optimizes the diode reverse recovery process and increases efficiency of the converter. The snubber capacitors C_S and C_{Sa} resonate with the leakage inductor L_{1k}. The capacitor C_S is charging, while the capacitor C_{Sa} is discharging. At t_4, the voltage across capacitor C_{Sa} resonates to zero. Because there is still a positive current on the leakage inductor L_{1k}, the body diode of switch S_a is conducted.

$$i_{L1k}(t) = \frac{V_S}{Z_1} \sin \omega_1 (t - t_3) - \frac{V_{S\,a}}{Z_1} \cos \omega_1 (t - t_3) - I_{in} \tag{4}$$

$$v_{CS}(t) = V_S \sin \omega_1 (t - t_3) \tag{5}$$

$$v_{CSa}(t) = V_{Sa} \sin \omega_1 (t - t_3) \tag{6}$$

where

$$\omega_1 = \frac{1}{\sqrt{(L_{1k} + L_m)(C_S + C_{Sa})}}, \quad Z_1 = \sqrt{\frac{L_{1k} + L_m}{C_S + C_{Sa}}}.$$

The interval duration of this mode is

$$t_4 - t_3 \geq 2\pi \sqrt{(L_{1k} + L_m)(C_S + C_{Sa})} \tag{7}$$

Mode *V* [t_4-t_5]. At t_4, the body diode of switch S turns on, the voltage across switch S is clamped to $V_{C1} + V_{C2}$ by capacitors C_1 and C_2, which decreases the voltage spike of switch S. Capacitor C_2 receives energy from input inductor L_1 as well as from input source V_g. The energy stored in magnetizing inductor L_m transferred to capacitor C_1, the magnetizing inductor current i_{Lm} decreases linearly.

Mode *VI* [t_5-t_6]. At t_5, the voltage across the switch Sa is clamped to zero results from conducted body diode. Thus, the switch S_a is turned on under zero-voltage condition. Input source V_g and input inductor L_1 release their energy to capacitor C_2. Magnetizing inductance L_m transfer its energy to capacitor C_1, L_m, capacitors C_3 and C_4 release their energy to load in series. Hence, the Magnetizing inductance current i_{Lm} decreases to zero. The diode D_o turns off under ZVZCS, which improves diode's reverse recovery characteristic.

Mode *VII* [t_6-t_7]. At t_6, the diodes D_1, D_2, and D_o are reverse biased. The magnetizing inductance current i_{Lm} reverse its direction, thus the stored energy in capacitor C_1 is transferred to magnetizing inductor L_m. The capacitor C_2 receives energy from input voltage V_g as well as from L_1 and C_1. The mode ends when control signal v_{GSa} changes from high level to low level.

III. STEADY-STATE ANALYSIS OF THE PROPOSED CONVERTER

Considering the duration of each Mode, only Mode III, Mode VI, and Mode VII are considered in the steady-state analysis of proposed converter. We assume that all the components of the converter are ideal and ignore the leakage inductance of the transformer.

A. VOLTAGE GAIN OF THE PROPOSED CONVERTER

Based on the aforementioned operating analysis in Mode III, the voltage across L_1 and the windings of the transformer can be expressed as:

$$\begin{cases} V_{L1\text{-}ON} = V_g + V_{C1} \\ V_{N1\text{-}ON} = V_{C2} \\ V_{N2\text{-}ON} = V_{C3} = V_{C4} \\ V_{N2\text{-}ON} = nV_{N1\text{-}ON} \end{cases} \tag{8}$$

where V_{L1-ON} is the voltage across L_1, V_{N1-ON} and V_{N2-ON} are the voltages on windings N_1 and N_2 during the ON state. V_{C1}, V_{C2}, V_{C3}, and V_{C4} is the voltage across the capacitors C_1, C_2, C_3, C_4, respectively. $n = N_2/N_1$, is the turn ratio of the transformer.

In Mode VI and Mode VII, the proposed converter obeys the same voltage equation.

$$\begin{cases} V_{L1\_OFF} = V_g - V_{C2} \\ V_{N1\_OFF} = -V_{C1} \\ V_{N2\_OFF} = V_{C4} + V_{C3} - V_{CO} \\ V_{N2\_OFF} = nV_{N1\_OFF} \end{cases} \tag{9}$$

where V_{L1-OFF} is the voltage across L_1, V_{N1-OFF} and V_{N2-OFF} are the voltages on windings N_1 and N_2 during the OFF state. V_{CO} is the output voltage of the converter, $n = N_2/N_1$ is the turn ratio of the transformer.

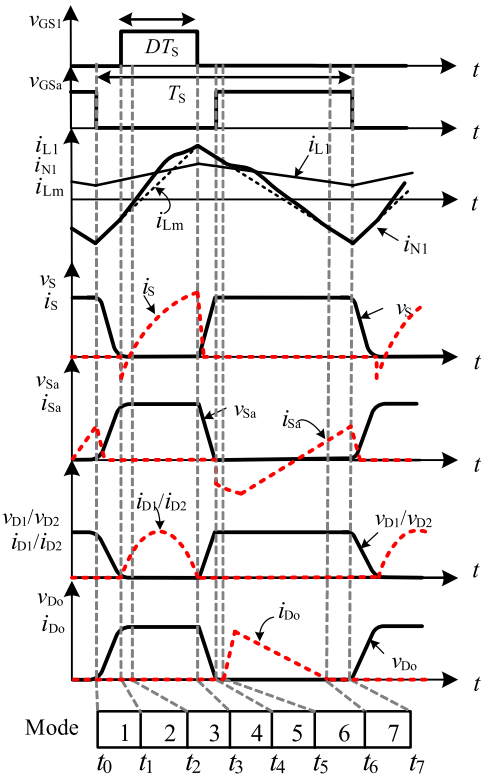

FIGURE 4. Key waveforms of the components.

Applying volt-second law on input inductor L_1 and windings of transformer, we have

$$\int_0^{DT_S} V_{i\text{-}ON} dt + \int_{DT_S}^{T_S} V_{i\text{-}OFF} dt = 0 \ (i = L_1, N_1, N_2) \tag{10}$$

On substituting (8) and (9) into (10), one has the voltage gain:

$$G = \frac{V_o}{V_g} = \frac{n(2-D)}{1-2D} \tag{11}$$

where V_o is the output voltage, D is the duty cycle.

The voltage gain G as a function of the duty ratio D is depicts in Fig. 6. The proposed converter has higher voltage gain at the appropriate small duty cycle.

B. STRESS ANALYSIS OF THE COMPONENTS

From (8) to (11), the voltage stress of the capacitors and devices are

$$\begin{cases} V_{C1} = \dfrac{D}{1-2D} V_g = \dfrac{D}{n(2-D)} V_o \\ V_{C2} = \dfrac{1-D}{1-2D} V_g = \dfrac{1-D}{n(2-D)} V_o \end{cases} \tag{12}$$

$$\begin{cases} V_{C3} = \dfrac{n(1-D)}{1-2D} V_g = \dfrac{1-D}{2-D} V_o \\ V_{C4} = \dfrac{n(1-D)}{1-2D} V_g = \dfrac{1-D}{2-D} V_o \end{cases} \tag{13}$$

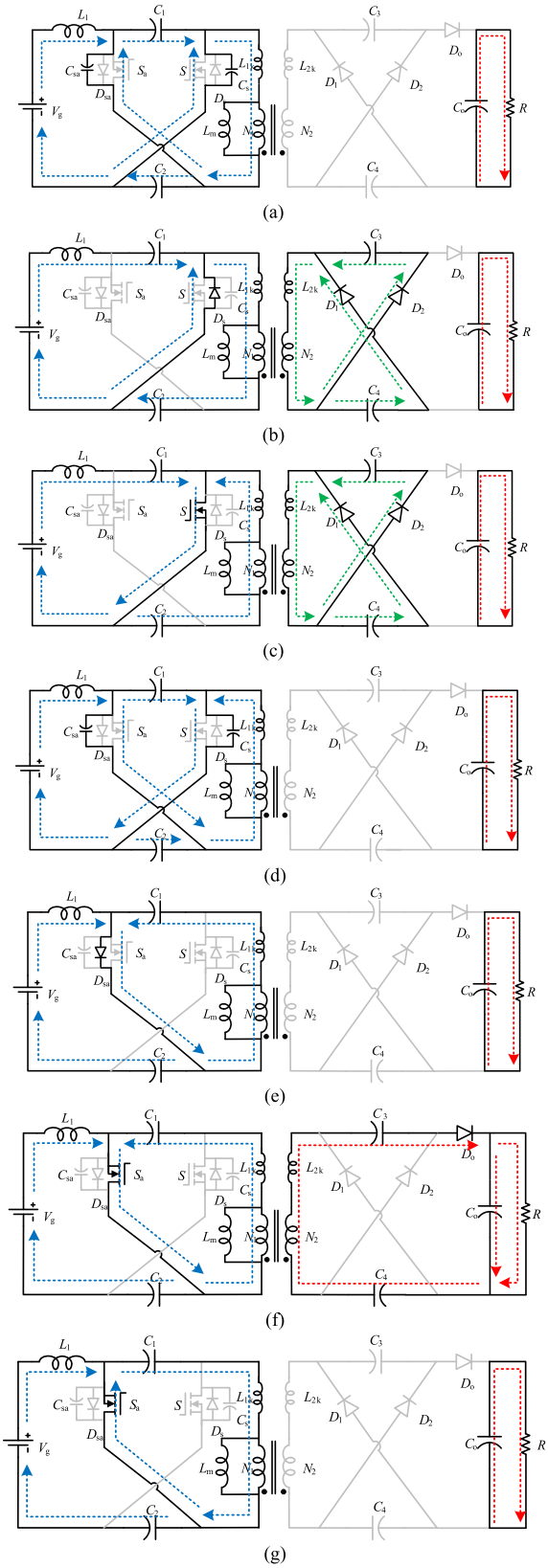

FIGURE 5. Operating modes of the proposed converter. (a) Mode I. (b) Mode II. (c) Mode III. (d) Mode IV. (e) Mode V. (f) Mode VI. (g) Mode VII.

$$V_{Co} = V_o = \frac{n(2-D)}{1-2D} V_g \tag{14}$$

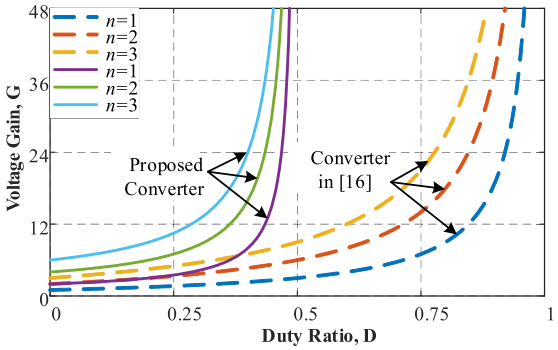

FIGURE 6. Voltage gain G as a function of the duty ratio D.

$$V_S = V_{Sa} = \frac{1}{1-2D} V_g = \frac{1}{n(2-D)} V_o \tag{15}$$

$$V_{D1} = V_{D2} = V_{DO} = \frac{n}{1-2D} V_g = \frac{1}{2-D} V_o \tag{16}$$

The current of the components in Mode III and Mode VI are expressed as

$$\begin{cases} I_{C1\_ON} = -I_{L1} \\ I_{C2\_ON} = I_{L1} - I_S \\ I_{C3\_ON} = I_{D2} \\ I_{C4\_ON} = I_{D1} - I_o - I_{CO\_ON} \\ I_{CO\_ON} = -I_o, \end{cases}$$
$$\begin{cases} I_{C1\_OFF} = I_{Sa} - I_{L1} \\ I_{C2\_OFF} = I_{L1} \\ I_{C3\_OFF} = -I_{Do} \\ I_{C4\_OFF} = -I_{CO\_OFF} - I_o \\ I_{CO\_OFF} = I_{DO} - I_o \end{cases} \tag{17}$$

where I_{Ci-ON} is the capacitor current during ON state. I_{Ci-OFF} is the current through capacitor C_i during OFF state. I_o is the output current of the converter.

Assuming that the converter has no power loss, the ampere-second law is applied to the capacitor C_i, and we can get

$$\begin{cases} I_{L1} = \dfrac{n(2-D)}{(1-2D)} I_o \\ \displaystyle\int_0^{DT} i_{Ci\_ON} dt + \int_{DT}^{T} i_{Ci\_OFF} dt = 0 (i = 1, 2, 3, 4, o) \end{cases} \tag{18}$$

Substituting (17) into (18), the current through switches and diodes are

$$\begin{cases} I_{DO} = \dfrac{1}{1-D} I_o, I_{D1} = \dfrac{1}{D} I_o, I_{D2} = \dfrac{1}{D} I_o \\ I_S = \dfrac{n(2-D)}{D(1-2D)} I_o, I_{Sa} = \dfrac{n(2-D)}{(1-D)(1-2D)} I_o \end{cases} \tag{19}$$

On substituting (19) into (17), we have

$$\begin{cases} I_{C1\_ON} = -\dfrac{n(2-D)}{1-2D} I_o \\ I_{C2\_ON} = \dfrac{n(D-1)(2-D)}{D(1-2D)} I_o \\ I_{C3\_ON} = \dfrac{1}{D} I_o \\ I_{C4\_ON} = \dfrac{1}{D} I_o \\ I_{CO\_ON} = -I_o \end{cases}$$

$$\begin{cases} I_{C1\_OFF} = \dfrac{Dn(2-D)}{(1-D)(1-2D)} I_o \\ I_{C2\_OFF} = \dfrac{n(2-D)}{1-2D} I_o \\ I_{C3\_OFF} = -\dfrac{1}{1-D} I_o \\ I_{C4\_OFF} = -\dfrac{1}{1-D} I_o \\ I_{CO\_OFF} = \dfrac{D}{1-D} I_o \end{cases} \tag{20}$$

The current stress on the windings of transformer is derived from Kirchhoff's Current Law (KCL) and ampere-second law. The average current of capacitor will be zero in one switching period.

$$I_{L1} = I_{Lm} + nI_o \tag{21}$$

Substituting (18) into (21), the current stress of the transformer is derived as

$$I\mathrm{Lm} = \frac{n(1+D)}{1-2D} I_o \tag{22}$$

C. EFFICIENCY ANALYSIS

The power loss of the proposed converter is consisted of the power dissipation of switches, diodes, capacitor, inductor, and transformer. An equivalent circuit of converter with parasitic resistance is shown in Fig. 7, where r_S is the switch on-resistance, r_D is the diode forward resistance, V_{FD} is the diode threshold voltage, r_{L1} is the ESR of the input inductor, r_N is the ESR of the winding, and r_C is the ESR of the capacitor.

The power dissipation of components is calculated with the method in [37]. Hence, the overall power loss of the proposed isolated converter can be described as

$$\begin{aligned} P_{Loss} &= P_{S\_loss} + P_{D\_loss} + P_{L\_Loss} + P_{C\_Loss} \\ &= r_{DS} \frac{n^2(2-D)^2 P_o}{D(1-2D)^2 R} + r_{DS} \frac{n^2(2-D)^2 P_o}{(1-D)(1-2D)^2 R} \\ &\quad + \frac{1}{6} \frac{f_s P_o}{D(1-2D)} (t_{on} \\ &\quad + t_{off}) + \frac{1}{6} \frac{f_s P_o}{(1-D)(1-2D)} (t_{on} + t_{off}) \\ &\quad + V_{FD1} \frac{1}{D} I_o + r_{D1} \frac{1}{D} I_o^2 + V_{FD2} \frac{1}{D} I_o + r_{D2} \frac{1}{D} I_o^2 + V_{FD0} I_o \end{aligned}$$

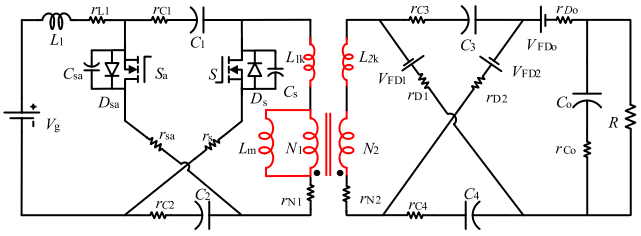

FIGURE 7. Operating modes of the proposed converter. (a) Mode I. (b) Mode II. (c) Mode III. (d) Mode IV. (e) Mode V. (f) Mode VI. (g) Mode VII.

$$\begin{aligned} &+ r_{D0} \frac{1}{1-D} I_o^2 + \frac{1}{6(2-D)} f_s I_{rr1} t_{b1} V_o \\ &+ \frac{1}{6(2-D)} f_s I_{rr2} t_{b2} V_o \\ &+ \frac{1}{6(2-D)} f_s I_{rr0} t_{b0} V_o + \frac{n^2(2-D)^2}{(1-2D)^2} \frac{r_{L1} P_o}{R} \\ &+ \frac{n^2(2-D)^2 (\frac{1}{D}-1)}{(1-2D)^2} \frac{r_{N1} P_o}{R} + \frac{4-3D}{D(1-D)} \frac{r_{N2} P_o}{R} \\ &+ r_{C1} \frac{P_o}{R} \frac{Dn^2(2-D)^2}{(1-2D)^2(1-D)} + r_{C2} \frac{P_o}{R} \frac{n^2(1-D)(2-D)^2}{D(1-2D)^2} \\ &+ r_{C3} \frac{P_o}{R} \frac{1}{D(1-D)} + r_{C4} \frac{P_o}{R} \frac{1}{D(1-D)} + r_{Co} \frac{P_o}{R} \frac{D}{1-D} \end{aligned} \tag{23}$$

where P_o is the output power, R is the load, P_{S-Loss}, P_{D-Loss}, P_{N-Loss}, P_{C-Loss} is the power loss of the switches, diodes, inductor/windings, and capacitors, respectively.

Fig. 8 depicts the efficiency η as function of the duty ratio with different output power P_o, at $r_S = 8$ mΩ, $t_{on+toff} = 41$ ns+64 ns = 144 ns, $V_{FD1} = V_{FD2} = 0.75$ V, $r_{D1} = r_{D2} = r_{DO} = 8$ mΩ, $t_{b1} = t_{b2} = t_{bo} = 40$ ns, $I_{rr} = 0.25$ A, $r_{L1} = 82$ mΩ, $r_{N1} = 2$ mΩ, $r_{N2} = 30$ mΩ, $r_{C1} = r_{C2} = 2$ mΩ, $r_{C3} = r_{C4} = 4.5$ mΩ, $r_{Co} = 9$ mΩ. It can be observed that the efficiency of proposed converter decreases as the duty cycle increases. The optimal range of the duty cycle D of the converter is $0.1 < D < 0.35$.

The power loss contribution of the different components is illustrated in Fig. 9 at voltage gain $G = 8$. In the total power loss, the magnetic elements power dissipation and active devices loss accounted for a relatively high proportion. It provides the theoretical basis for the efficiency optimization design of the converter. Soft switching technique used in proposed converter significantly reduces power loss.

IV. DESIGN GUIDELINES

The theoretical parameters design of the proposed converter is based on the input voltage of 48 V, the output voltage of 400 V, and the rated power of 200 W.

A. ZVS OPERATION OF THE POWER SWITCH

Leakage inductance and snubber capacitor resonance provide zero-voltage switching condition of the switches and zero-voltage zero-current switching of the diodes in the proposed converter.

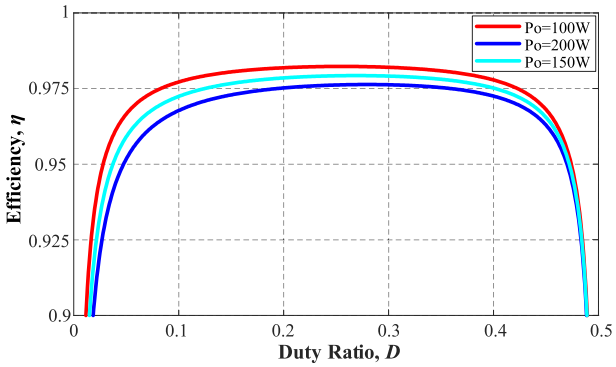

FIGURE 8. Calculated efficiency versus duty ratio D at turns ratio n = 2.

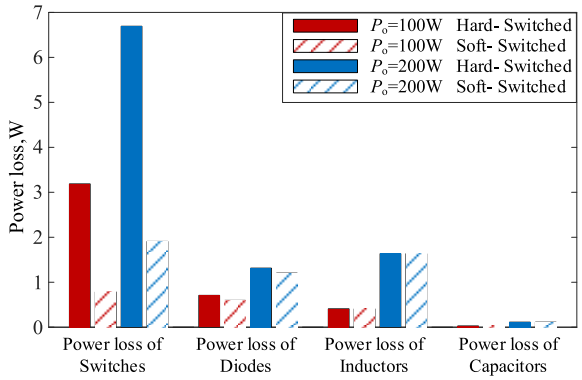

FIGURE 9. Calculated power loss distribution of the components at G = 8 in Soft/Hard switched condition at 100 W and 200 W.

From Fig. 5, we obtain (24) with KCL during Mode I, which is

$$i_S + i_{Sa} = -i_{Lm} - i_{L1} \tag{24}$$

In Mode IV, the current flown through the switches are

$$i_S + i_{Sa} = i_{Lm} + i_{L1} \tag{25}$$

In Mode I, the snubber capacitors C_S and C_{Sa} are resonant with the leakage inductor L1k, the capacitor C_S is discharged, and the capacitor C_{Sa} is charged. In order to achieve soft switching condition, the snubber capacitor C_{Sa} and C_S must be fully charged and discharged in one switching period. Thus, we have

$$-i_{Lm\text{-}t0} - i_{L1\text{-}t0} > 0 \tag{26}$$

where i_{L1-T0}, i_{Lm-T0} is the inductor current and magnetizing inductor current at t_0, respectively.

Fig. 10 shows the waveforms of the input inductor current i_{L1}, magnetizing inductor current i_{Lm}, and winding current i_{N1}. In this converter, the ripple of input inductor current i_{L1} is very small compared to that of magnetizing inductor current i_{Lm}. Therefore, for simplicity, we assume that the input inductor current is constant during a switching period. From Fig. 8, the magnetizing inductor current at t_0 can be

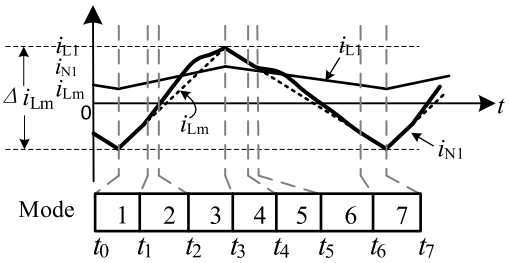

FIGURE 10. Waveforms of the input inductor current iL1, magnetizing inductor current iLm, and winding current iN1.

written as

$$i_{Lm\text{-}t0} = I_{Lm} - \frac{1}{2}\Delta i_{Lm} \tag{27}$$

On substituting (27) into (26), one has

$$\Delta i_{Lm} > 2(I_{L1} + I_{Lm}) \tag{28}$$

where Δi_{Lm} is the magnetizing inductor current increase during the on state.

The equation for magnetizing inductor can be expressed as

$$L_m = \frac{V_{Lm}D}{f_S \Delta i_{Lm}} = \frac{V_{C2}D}{f_S \Delta i_{Lm}} \tag{29}$$

where f_s is the switching frequency.

Upon equating Δi_{Lm} from (28), and then solving for L_m, then

$$L_m < \frac{(1-D)(1-2D)DR}{6f_S n^2(2-D)} \tag{30}$$

The selection of snubber capacitors C_S and C_{Sa} must meet the energy requirements of soft switching of converter. The equivalent inductance L_{eq} of L_1 and L_m in parallel must have an energy greater than that required by the snubber capacitors. It may be shown that

$$0.5L_{eq}i^2_{Leq\text{-}t0} > 0.5(C_S + C_{Sa})(V_{C1} + V_{C2})^2 \tag{31}$$

where i_{Leq-t0} is the equivalent inductor current at t_0.

From Fig. 10, the equivalent inductor current is given by

$$i_{Leq\text{-}t0} = i_{in\text{-}t0} + i_{Lm\text{-}t0} = I_{L1} + (I_{Lm} - 0.5\Delta i_{Lm}) \tag{32}$$

Substituting (32) into (31), the snubber capacitor design criterion is

$$C_{S,Sa} < \frac{L_{eq}}{2}\left(\frac{I_{L1} + I_{Lm} - 0.5\Delta i_{Lm}}{V_{C1} + V_{C2}}\right)^2 \tag{33}$$

The realization of ZVZCS of diodes D_1 and D_2 depends entirely on the values of capacitors C_3, C_4 and the leakage inductance L_{2k}. The duration of the on state must be slightly longer than half of the resonant period, which is

$$t_3 - t_1 = DT_S > \frac{T_0}{2} = \pi\sqrt{L_{2k}(C_3 + C_4)} \tag{34}$$

The capacitor $C_{3,4}$ can be represented as

$$C_{3,4} < \frac{1}{2L_{2k}}\left(\frac{D}{\pi f_S}\right)^2 \tag{35}$$

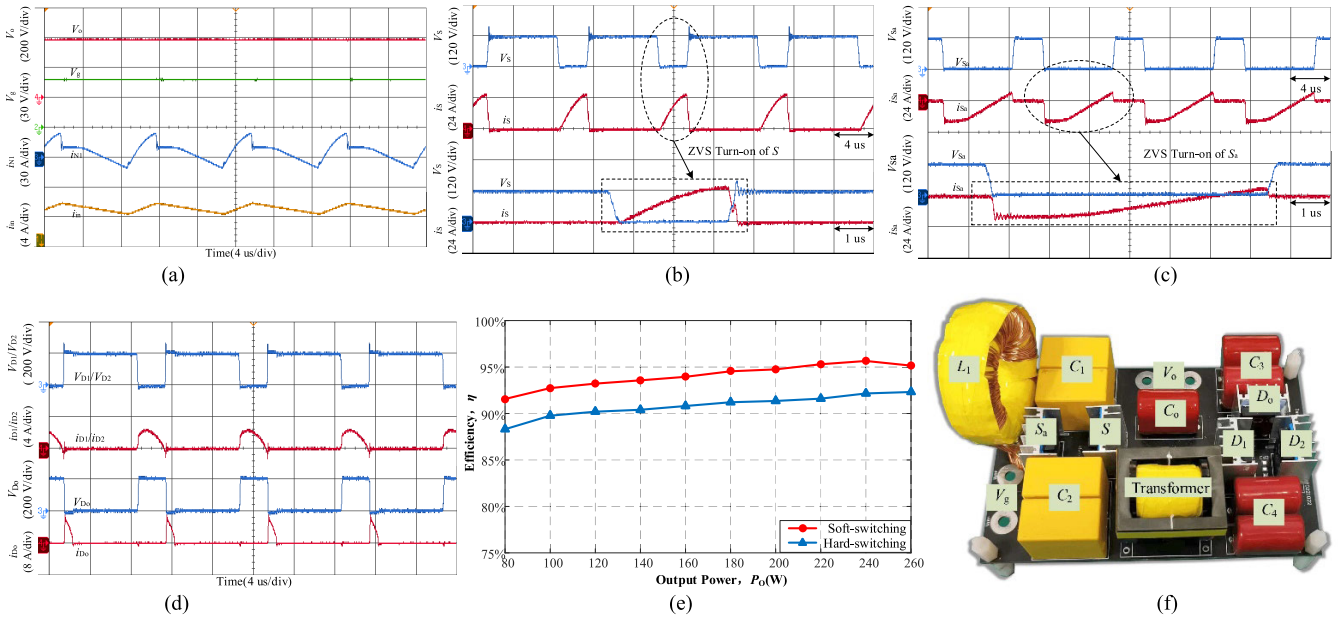

FIGURE 11. Experimental results at Po = 200 W. (a) Output voltage, input voltage, magnetizing inductance current and Input current. (b) Main switch S. (c) Auxiliary switch Sa. (d) Diode D1, D2 and Output diode Do. (e) Measured efficiency of the proposed converter (G = 8). (f) Photo of the proposed converter.

B. PARAMETER DESIGN

1) INPUT INDUCTOR DESIGN

The input inductor can be expressed as

$$L_1 = \frac{V_{\text{L-on}}\Delta t}{\Delta i_{\text{L1}}} = \frac{V_{\text{L-on}}D}{f_s \Delta i_{\text{L1}}} \tag{36}$$

Where Δi_{L1} is the input inductor current ripple during the on state, $\Delta i_{\text{L1}} = r_{\text{L}} I_{\text{L1}}$, $0.15 < r_{\text{L}} < 0.2$. I_{L1} is the input inductor current average value.

From (8), (11), and (18), we have

$$V_{\text{L-on}} = \frac{1-D}{1-2D} V\text{g} = \frac{1-D}{n(2-D)} V_{\text{O}},\ I_{\text{L1}} = \frac{n(2-D)}{(1-2D)} I_{\text{o}} \tag{37}$$

Substituting this term for $V_{\text{L-on}}$ and I_{L1} in (36) yields the following equation.

$$L_1 \geq \frac{(1-D)(1-2D)DR}{n^2(2-D)^2 f_s r_{\text{L}}} \tag{38}$$

where R is the load.

2) TRANSFORMER DESIGN

The transformer is designed by A_{P} method [38], we have the window-cross-section product A_{p}.

$$A_{\text{P}} = A_{\text{c}} W_{\text{a}} = \frac{P_{\text{t}} \times 10^4}{J k_{\text{u}} k_{\text{f}} B_{\max} f_s} = \frac{V_{\text{N1\_ON}} I_{\text{N1\_ON}} \times 10^4}{J k_{\text{u}} k_{\text{f}} B_{\max} f_s} \tag{39}$$

where A_{c} is the cross-sectional area of the magnetic core. W_{a} is the window area of the core. P_{t} is the apparent power of the transformer. J is the current density in each winding. k_{u} is the window utilization factor, $k_{\text{u}} = 0.35$. kf is the core stacking factor, $k_{\text{f}} = 4$. $B_{\max}$ is the maximum value of flux density, $B_{\max} = 0.25$T.

Finally, EC35 core was selected according to A_{p} calculation results and considering the margin. Thus, the number of turns of the transformer's windings N_{p}, N_{s} are

$$\begin{cases} N_{\text{p}} = \dfrac{V_{\text{N1-ON}} D}{A_{\text{c}} \times \Delta B \times f_s} \\ N_{\text{s}} = n N_{\text{p}} \end{cases} \tag{40}$$

where ΔB is the flux density variation during the on state.

V. EXPERIMENTAL RESULTS

The laboratory prototype is destructed to demonstrate the validity and practicability of the proposed isolated converter. The system experiment environment and parameters are as follows:

1) input dc voltage V_{g}: 48 V;
2) output dc voltage V_{o}: 380 V;
3) rated output power P_{o}: 200 W;
4) frequency f: 100 kHz;
5) input inductor L_{in}: 360 μH, coupled-inductor: $N_{\text{p}} = 6$, $N_{\text{s}} = 12$;
6) switches: IRFP4668PbF; diodes: STTH6003CW.

Fig. 11 are the results of the proposed isolated dc-dc converter with rated output power 200 W. The input voltage and output voltage waveforms are shown in Fig. 9(a), which fits very well with theoretical calculation $Vo = 2(2\text{-}D)/(1\text{-}2D)$. The input current i_{in} is continuous, as shown in Fig. 11(a).

The switch S is turn on with zero voltage switching (shown in Fig. 11(b)), and the auxiliary switch S_{a} is also turn on with zero voltage switching, as Fig. 11(c) shows. The diodes

are turn off with zero current switching, which decreases the power loss of diode reverse recovery. The voltage and current waveforms of diodes are shown in Fig. 11(d).

The measured efficiency of proposed converter versus output power with $G = 8$ is depicted in Fig. 11(e). The efficiency of the converter with soft-switching is 3 to 4 % higher than that in hard switching transition.

VI. CONCLUSION

A high efficiency, high step-up, isolated soft-switching PWM quasi-Z-source dc-dc converter with a low component count was presented. The proposed converter was able to provide very high voltage gain, along with low input current ripple. Turn-on ZVS can be achieved for main and auxiliary switches, and turn-on and turn-off ZVZCS transition can be realized for all the diodes. The leakage inductance energy is recycled by the active clamp circuit inherent in the quasi-Z source network, thus the voltage spike across the switches is suppressed. The voltage spike of the diodes is eliminated due to the ZVZCS turn-off. The peak efficiency reaches 95.6% at 240 W ($G = 8$), and 95.1% at 260 W.

REFERENCES

[1] F. P. Hartwell, J. F. McPartland, and B. J. McPartland, *National Electrical Code 2017 Handbook (NEC)*, 29th ed. New York, NY, USA: McGraw-Hill, 2017, ch. 6, pp. 1495–1515.

[2] I. Patrao, E. Figueres, G. Garcerá, and R. González-Medina, "Microgrid architectures for low voltage distributed generation," *Renew. Sustain. Energy Rev.*, vol. 43, pp. 415–424, Mar. 2015, doi: 10.1016/j.rser.2014.11.054.

[3] M. Forouzesh, Y. Shen, K. Yari, Y. P. Siwakoti, and F. Blaabjerg, "High-efficiency high step-up DC–DC converter with dual coupled inductors for grid-connected photovoltaic systems," *IEEE Trans. Power Electron.*, vol. 33, no. 7, pp. 5967–5982, Jul. 2018, doi: 10.1109/TPEL.2017.2746750.

[4] C. M. N. Mukundan, S. B. Q. Naqvi, Y. Singh, B. Singh, and P. Jayaprakash, "A cascaded generalized integral control for multi-objective grid-connected solar energy transfer system," *IEEE Trans. Ind. Electron.*, vol. 68, no. 12, pp. 12385–12395, Dec. 2021, doi: 10.1109/TIE.2020.3048316.

[5] Y. Zhuang, F. Liu, Y. Huang, S. Wang, S. Pan, X. Zha, and X. Diao, "A multiport DC solid-state transformer for MVDC integration interface of multiple distributed energy sources and DC loads in distribution network," *IEEE Trans. Power Electron.*, vol. 37, no. 2, pp. 2283–2296, Feb. 2022, doi: 10.1109/TPEL.2021.3105528.

[6] A. Kulkarni, A. Gupta, and S. K. Mazumder, "Resolving practical design issues in a single-phase grid-connected GaN-FET-based differential-mode inverter," *IEEE Trans. Power Electron.*, vol. 33, no. 5, pp. 3734–3751, May 2018, doi: 10.1109/TPEL.2017.2767572.

[7] C. A. Rojas, S. Kouro, M. A. Perez, and J. Echeverria, "DC–DC MMC for HVdc grid interface of utility-scale photovoltaic conversion systems," *IEEE Trans. Ind. Electron.*, vol. 65, no. 1, pp. 352–362, Jan. 2018, doi: 10.1109/TIE.2017.2714120.

[8] Y.-E. Wu and Y.-T. Ke, "A novel bidirectional isolated DC–DC converter with high voltage gain and wide input voltage," *IEEE Trans. Power Electron.*, vol. 36, no. 7, pp. 7973–7985, Jul. 2021, doi: 10.1109/TPEL.2020.3045986.

[9] V. K. Goyal and A. Shukla, "Isolated DC–DC boost converter for wide input voltage range and wide load range applications," *IEEE Trans. Ind. Electron.*, vol. 68, no. 10, pp. 9527–9539, Oct. 2021, doi: 10.1109/TIE.2020.3029479.

[10] X. Pan, H. Li, Y. Liu, T. Zhao, C. Ju, and A. K. Rathore, "An overview and comprehensive comparative evaluation of current-fed-isolated-bidirectional DC/DC converter," *IEEE Trans. Power Electron.*, vol. 35, no. 3, pp. 2737–2763, Mar. 2020, doi: 10.1109/TPEL.2019.2931739.

[11] N. Hou and Y. W. Li, "Overview and comparison of modulation and control strategies for a nonresonant single-phase dual-active-bridge DC–DC converter," *IEEE Trans. Power Electron.*, vol. 35, no. 3, pp. 3148–3172, Mar. 2020, doi: 10.1109/TPEL.2019.2927930.

[12] T.-T. Nguyen, H. Cha, and H.-G. Kim, "Current-fed quasi-Z-source full-bridge isolated DC–DC converter," *IEEE Trans. Ind. Electron.*, vol. 68, no. 12, pp. 12046–12057, Dec. 2021, doi: 10.1109/TIE.2020.3047008.

[13] Y. Zhu, Z. Guo, and Q. Geng, "An improved full-bridge converter with a five-diode rectifier for high efficiency in wide voltage range," *IEEE Trans. Power Electron.*, vol. 37, no. 3, pp. 3178–3191, Mar. 2022, doi: 10.1109/TPEL.2021.3109939.

[14] Y. Jeong, M.-S. Lee, J.-D. Park, J.-K. Kim, and Ronald. A. L. Rorrer, "Hold-up time compensation circuit of half-bridge LLC resonant converter for high light-load efficiency," *IEEE Trans. Power Electron.*, vol. 35, no. 12, pp. 13126–13135, Dec. 2020, doi: 10.1109/TPEL.2020.2992751.

[15] N. C. D. Pont, D. G. Bandeira, T. B. Lazzarin, and I. Barbi, "A ZVS APWM half-bridge parallel resonant DC–DC converter with capacitive output," *IEEE Trans. Ind. Electron.*, vol. 66, no. 7, pp. 5231–5241, Jul. 2019, doi: 10.1109/TIE.2018.2868270.

[16] J.-H. Lee, T.-J. Liang, and J.-F. Chen, "Isolated coupled-inductor-integrated DC–DC converter with nondissipative snubber for solar energy applications," *IEEE Trans. Ind. Electron.*, vol. 61, no. 7, pp. 3337–3348, Jul. 2014, doi: 10.1109/TIE.2013.2278517.

[17] E. Serban, M. A. Saket, and M. Ordonez, "High-performance isolated gate-driver power supply with integrated planar transformer," *IEEE Trans. Power Electron.*, vol. 36, no. 10, pp. 11409–11420, Oct. 2021, doi: 10.1109/TPEL.2021.3070053.

[18] J. Lee, M. Kim, S. Kim, and S. Choi, "An isolated single-switch ZCS resonant converter with high step-up ratio," *IEEE Trans. Power Electron.*, vol. 36, no. 10, pp. 11555–11564, Oct. 2021, doi: 10.1109/TPEL.2021.3072647.

[19] N. M. Mukhtar and D. D. Lu, "A bidirectional two-switch flyback converter with cross-coupled LCD snubbers for minimizing circulating current," *IEEE Trans. Ind. Electron.*, vol. 66, no. 8, pp. 5948–5957, Aug. 2019, doi: 10.1109/TIE.2018.2873097.

[20] T. Qian and Q. Wu, "A scheme of a resonant forward-flyback converter with suppressed frequency variation," *IEEE Trans. Power Electron.*, vol. 33, no. 5, pp. 3711–3716, May 2018, doi: 10.1109/TPEL.2017.2766024.

[21] S. Sathyan, H. M. Suryawanshi, A. B. Shitole, M. S. Ballal, and V. B. Borghate, "Soft-switched interleaved DC/DC converter as front-end of multi-inverter structure for micro grid applications," *IEEE Trans. Power Electron.*, vol. 33, no. 9, pp. 7645–7655, Sep. 2018, doi: 10.1109/TPEL.2017.2768379.

[22] P. Gunawardena, D. Nayanasiri, N. Hou, and Y. Li, "A soft-switched current-fed dual-input isolated DC–DC converter topology," *IEEE Trans. Ind. Electron.*, vol. 70, no. 5, pp. 4842–4853, May 2023, doi: 10.1109/TIE.2022.3190878.

[23] K.-C. Tseng, S.-Y. Chang, and C.-A. Cheng, "Novel isolated bidirectional interleaved converter for renewable energy applications," *IEEE Trans. Ind. Electron.*, vol. 66, no. 12, pp. 9278–9287, Dec. 2019, doi: 10.1109/TIE.2019.2892673.

[24] S.-W. Lee and H.-L. Do, "Isolated SEPIC DC–DC converter with ripple-free input current and lossless snubber," *IEEE Trans. Ind. Electron.*, vol. 65, no. 2, pp. 1254–1262, Feb. 2018, doi: 10.1109/TIE.2017.2733440.

[25] Z. Wang, Z. Zheng, and C. Li, "A high-step-up low-ripple and high-efficiency DC–DC converter for fuel-cell vehicles," *IEEE Trans. Power Electron.*, vol. 37, no. 3, pp. 3555–3569, Mar. 2022, doi: 10.1109/TPEL.2021.3112072.

[26] A. Elkhateb, N. A. Rahim, J. Selvaraj, and B. W. Williams, "DC-to-DC converter with low input current ripple for maximum photovoltaic power extraction," *IEEE Trans. Ind. Electron.*, vol. 62, no. 4, pp. 2246–2256, Apr. 2015, doi: 10.1109/TIE.2014.2383999.

[27] S. S. Dobakhshari, S. H. Fathi, and J. Milimonfared, "A new soft-switched three-port DC/DC converter with high voltage gain and reduced number of semiconductors for hybrid energy applications," *IEEE Trans. Power Electron.*, vol. 35, no. 4, pp. 3590–3600, Apr. 2020, doi: 10.1109/TPEL.2019.2933182.

[28] B. Zhu, H. Wang, Y. Zhang, and S. Chen, "Buck-based active-clamp circuit for current-fed isolated DC–DC converters," *IEEE Trans. Power Electron.*, vol. 37, no. 4, pp. 4337–4345, Apr. 2022, doi: 10.1109/TPEL.2021.3121704.

[29] S.-H. Lee, B.-S. Lee, D.-H. Kwon, J.-H. Ahn, and J.-K. Kim, "Two-mode low-voltage DC/DC converter with high and wide input voltage range," *IEEE Trans. Ind. Electron.*, vol. 68, no. 12, pp. 12088–12099, Dec. 2021, doi: 10.1109/TIE.2020.3039214.
[30] I.-B. Kong, W.-S. Kim, and S.-W. Lee, "A novel high-voltage-gain quasi-resonant DC–DC converter with active-clamp and switched-capacitor techniques," *IEEE Trans. Power Electron.*, vol. 38, no. 6, pp. 7810–7820, Jun. 2023, doi: 10.1109/TPEL.2023.3259012.
[31] B. Wu, S. Li, and K. Ma Smedley, "A new single-switch isolated high-gain hybrid boosting converter," *IEEE Trans. Ind. Electron.*, vol. 63, no. 8, pp. 4978–4988, Aug. 2016, doi: 10.1109/TIE.2016.2554542.
[32] H. Tarzamni, E. Babaei, and A. Z. Gharehkoushan, "A full soft-switching ZVZCS flyback converter using an active auxiliary cell," *IEEE Trans. Ind. Electron.*, vol. 64, no. 2, pp. 1123–1129, Feb. 2017, doi: 10.1109/TIE.2016.2615601.
[33] C. Wang, S. Xu, W. Shen, S. Lu, and W. Sun, "A single-switched high-switching-frequency quasi-resonant flyback converter," *IEEE Trans. Power Electron.*, vol. 34, no. 9, pp. 8775–8786, Sep. 2019, doi: 10.1109/TPEL.2018.2884937.
[34] L. Chang, T. Guo, J. Liu, C. Zhang, Y. Deng, and X. He, "Analysis and design of a current-source CLCC resonant converter for DBD applications," *IEEE Trans. Power Electron.*, vol. 29, no. 4, pp. 1610–1621, Apr. 2014, doi: 10.1109/TPEL.2013.2266376.
[35] L. Zheng, R. P. Kandula, and D. Divan, "Current-source solid-state DC transformer integrating LVDC microgrid, energy storage, and renewable energy into MVDC grid," *IEEE Trans. Power Electron.*, vol. 37, no. 1, pp. 1044–1058, Jan. 2022, doi: 10.1109/TPEL.2021.3101482.
[36] K. Zaoskoufis and E. C. Tatakis, "Isolated ZVS-ZCS DC–DC high step-up converter with low-ripple input current," *IEEE J. Emerg. Sel. Topics Ind. Electron.*, vol. 2, no. 4, pp. 464–480, Oct. 2021, doi: 10.1109/JESTIE.2021.3063913.
[37] X. Ding, F. Wang, M. Zhou, Y. Cao, and Z. Wei, "Soft switching high voltage gain quasi-Z-source DC–DC converter with switched-capacitor technique," *IEEE Trans. Ind. Electron.*, vol. 69, no. 11, pp. 11231–11241, Nov. 2022, doi: 10.1109/TIE.2021.3125649.
[38] P. Mohseni, S. H. Hosseini, and M. Maalandish, "A new soft switching DC–DC converter with high voltage gain capability," *IEEE Trans. Ind. Electron.*, vol. 67, no. 9, pp. 7386–7398, Sep. 2020, doi: 10.1109/TIE.2019.2941130.

GUOSHENG TIAN received the B.Eng. and M.Eng. degrees from Liaoning Technical University, Liaoning, China, in 1999 and 2007, respectively.

He is currently an Associate Professor and a Master Supervisor with Liaoning Technical University. His main research interests include smart grid new technology, high-voltage gain dc–dc converters, and high-voltage dc transmission (HVdc).

SHUO CHEN was born in Henan, China, in 1999. He received the B.S. degree in smart grid information engineering from Liaoning Technical University, Liaoning, China, in 2021, where he is currently pursuing the M.Sc. degree in control theory and control engineering.

His research interests include high step-up dc–dc converters, power electronics, and soft switching techniques.

XINPING DING (Member, IEEE) was born in Dingxi, China. He received the Ph.D. degree in electrical engineering from the College of Electrical Engineering, Zhejiang University, Hangzhou, China, in 2007.

From 2007 to 2020, he was a Faculty Member with Qingdao University of Technology. Since January 2021, he has been a Faculty Member with Nanjing University of Information Science and Technology, where he is currently a Full Professor with the School of Automation. He has coauthored over 50 papers and holds five patents. His research interests include power converters for Z-source inverters, renewable energy systems, and high voltage gain high-efficiency dc–dc converters. He serves as a Reviewer for IEEE TRANSACTIONS ON INDUSTRIAL ELECTRONICS, IEEE TRANSACTIONS ON POWER ELECTRONICS, and *IET Power Electronics*.

JISHEN PENG received the bachelor's degree from Xi'an Jiaotong University, in 1991, and master's degree from Liaoning Technical University, in 1998.

He is currently a Professor and a Ph.D. Supervisor with Liaoning Technical University. His main research interests include industrial process control and optimization.

ZHUANGZHUANG KOU was born in Jiangsu, China, in 1999. He received the B.S. degree in measurement and control technology and instrumentation from Nanjing Institute of Technology, Nanjing, China, in 2021. He is currently pursuing the M.S. degree in electronic information with Nanjing University of Information Science and Technology.

His research interests include power electronics topology, high-voltage gain dc–dc converters, and soft-switching techniques.